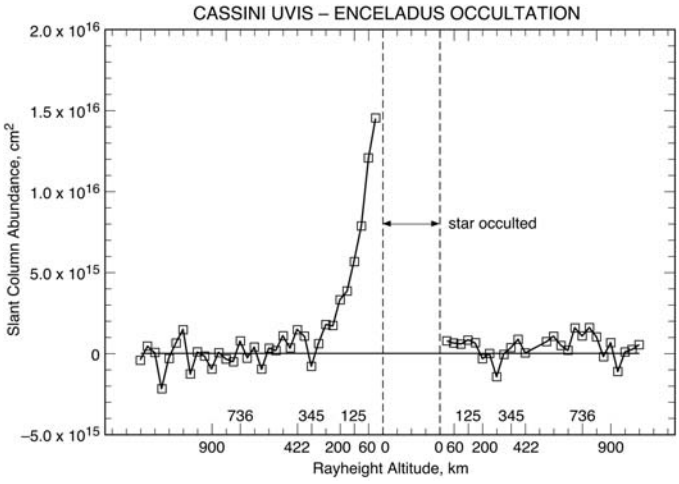


**Fig. 5.** Water abundance shown as a function of time (ticks are every 10 s), labeled with the ray height in kilometers at a few representative times.

tends from about three to at least eight Saturn radii, with a peak density at Enceladus' orbit (*2*). Analysis by Jurac *et al.* (*16*) concluded that the lifetimes of 1-μm grains are <50 years, because water molecules are sputtered from the grains' surfaces by the plasma trapped in Saturn's magnetosphere. A source of water is needed to maintain the E ring.

Saturn's system is filled with neutral products from the electron- and photodissociation of $H_2O$ molecules: Hubble Space Telescope observations detected neutral OH (*17*), and UVIS detected neutral atomic oxygen throughout Saturn's system (*18*) as the Cassini spacecraft approached Saturn. Most $H_2O$ molecules dissociate to H + OH, with more O coming from the subsequent dissociation of OH. Neutrals are lost from the system because of charge exchange and collisions with ions. From measured O and OH abundances and theoretical estimates of the loss processes of all water products from the system, various investigators have estimated $H_2O$ supply rates necessary to maintain a steady state as $>2 \times 10^{27}$ $H_2O$ molecules/s (*17*), possibly as high as $3.75 \times 10^{27}$ (*19*) or $10^{28}$ $H_2O$ molecules/s (*20*, *21*). Potential $H_2O$ sources identified by these investigators included sputtering and collisions; however, the rates of these processes are not sufficient to replace the lost neutrals (*19*). The source for resupplying the E ring and replacing the neutrals remained a mystery until the discovery of the water vapor plume coming from Enceladus.

The inferred source rate of $H_2O$ in the present observation is of the same order as the earlier estimated loss rates for O and OH. If Enceladus is responsible for the majority of water product gas in the magnetosphere, this implies eruptive activity over at least the past 15 years. The escape flux of water from Enceladus' plume calculated from our measurement of the column density may or may not represent a steady state, because the observation history is confined to a single flyby. Based simply on source magnitude, however, it is probable that Enceladus is the dominant source of the observed neutrals in the Saturn system.

If Enceladus is a significant source for maintaining the E ring, it implies that grain particles are part of the mix of matter in the plume. If Enceladus' plume has a comet-like dust-to-gas ratio, then the mass of water coming from Enceladus, >150 kg/s, is more than sufficient to compensate for the estimated loss rate of the E ring of 1 kg/s (*22*). The polar plume at Enceladus is clearly an unusual and important geophysical phenomenon.

### References and Notes


1. B. A. Smith *et al.*, *Science* **215**, 504 (1982).
2. M. R. Showalter, J. N. Cuzzi, S. M. Larson, *Icarus* **94**, 451 (1991).
3. R. J. Terrile, A. Cook, *Lunar Planet. Sci* **12** (suppl. A), 10 (1981).
4. B. J. Buratti, *Icarus* **75**, 113 (1988).
5. M. Horanyi, J. A. Burns, D. P. Hamilton, *Icarus* **97**, 248 (1992).
6. L. Esposito *et al.*, *Space Sci. Rev.* **115**, 299 (2004).
7. M. K. Dougherty *et al.*, *Science* **311**, 1406 (2006).
8. J. Saur, D. F. Strobel, *Astrophys. J.* **620**, L115 (2005).
9. G. R. Smith, D. M. Hunten, *Rev. Geophys.* **28**, 117 (1990).
10. W. F. Chan, G. Cooper, C. E. Brion, *Chem. Phys.* **178**, 387 (1993).
11. R. Harrevelt, M. C. Hemert, *J. Chem. Phys.* **114**, 9453 (2001).
12. J. H. Waite Jr. *et al.*, *Science* **311**, 1419 (2006).
13. M. Eidelsberg, F. Rostas, J. Breton, B. Thieblemont, *J. Chem. Phys.* **96**, 5585 (1992).
14. J. R. Spencer *et al.*, *Science* **311**, 1401 (2006).
15. P. D. Nicholson *et al.*, *Science* **272**, 509 (1996).
16. S. Jurac, R. E. Johnson, J. D. Richardson, *Icarus* **149**, 384 (2001).
17. D. P. Shemansky Matheson, D. T. Hall, H.-Y. Hu, T. M. Tripp, *Nature* **363**, 329 (1993).
18. L. W. Esposito *et al.*, *Science* **307**, 1251 (2005).
19. S. Jurac *et al.*, *Geophys. Res. Lett.* **29**, 2172 (2002).
20. S. Jurac, J. D. Richardson, *J. Geophys. Res.* **110**, A09220 (2005).
21. D. Shemansky *et al.*, paper presented at the meeting of the Committee on Space Research, Paris, France, 18 July 2004.
22. A. Juhasz, M. Horanyi, *J. Geophys. Res.* **107**, 1066 (2002).


23. This work was partially supported by the Jet Propulsion Laboratory, California Institute of Technology, under a contract with NASA. We thank N. Strange for his efforts in ensuring that the gamma Orionis occultation was included in the design of Cassini's trajectory past Enceladus.


**Supporting Online Material**

www.sciencemag.org/cgi/content/full/311/5766/1422/DC1
Fig. S1

12 October 2005; accepted 20 January 2006
10.1126/science.1121254

REPORT

# Composition and Physical Properties of Enceladus' Surface

**Robert H. Brown,[1] Roger N. Clark,[2] Bonnie J. Buratti,[3] Dale P. Cruikshank,[4] Jason W. Barnes,[1] Rachel M. E. Mastrapa,[4] J. Bauer,[3] S. Newman,[3] T. Momary,[3] K. H. Baines,[3] G. Bellucci,[5] F. Capaccioni,[6] P. Cerroni,[6] M. Combes,[7] A. Coradini,[6] P. Drossart,[7] V. Formisano,[5] R. Jaumann,[8] Y. Langevin,[9] D. L. Matson,[3] T. B. McCord,[10] R. M. Nelson,[3] P. D. Nicholson,[11] B. Sicardy,[7] C. Sotin[12]**

Observations of Saturn's satellite Enceladus using Cassini's Visual and Infrared Mapping Spectrometer instrument were obtained during three flybys of Enceladus in 2005. Enceladus' surface is composed mostly of nearly pure water ice except near its south pole, where there are light organics, $CO_2$, and amorphous and crystalline water ice, particularly in the region dubbed the "tiger stripes." An upper limit of 5 precipitable nanometers is derived for CO in the atmospheric column above Enceladus, and 2% for $NH_3$ in global surface deposits. Upper limits of 140 kelvin (for a filled pixel) are derived for the temperatures in the tiger stripes.

Saturn's sixth largest satellite, Enceladus, orbits the planet within the extended E ring at a distance of 238,040 km, or ~4 Saturn radii. Enceladus has an equatorial diameter of 504.2 km and a surface that consists of a composite of moderately cratered terrain and large expanses with no craters (*1*). Internal activity has resulted in several episodes of resurfacing, ridge building, folding, and faulting (*2*, *3*). Near-infrared spectroscopy of Enceladus from Earth-based telescopes (*4*–*6*) has revealed partially crystalline $H_2O$ ice, consistent with Enceladus' unusually high reflectance. At wavelength 0.8 μm, the geometric albedo slightly exceeds 1.0 (*5*).

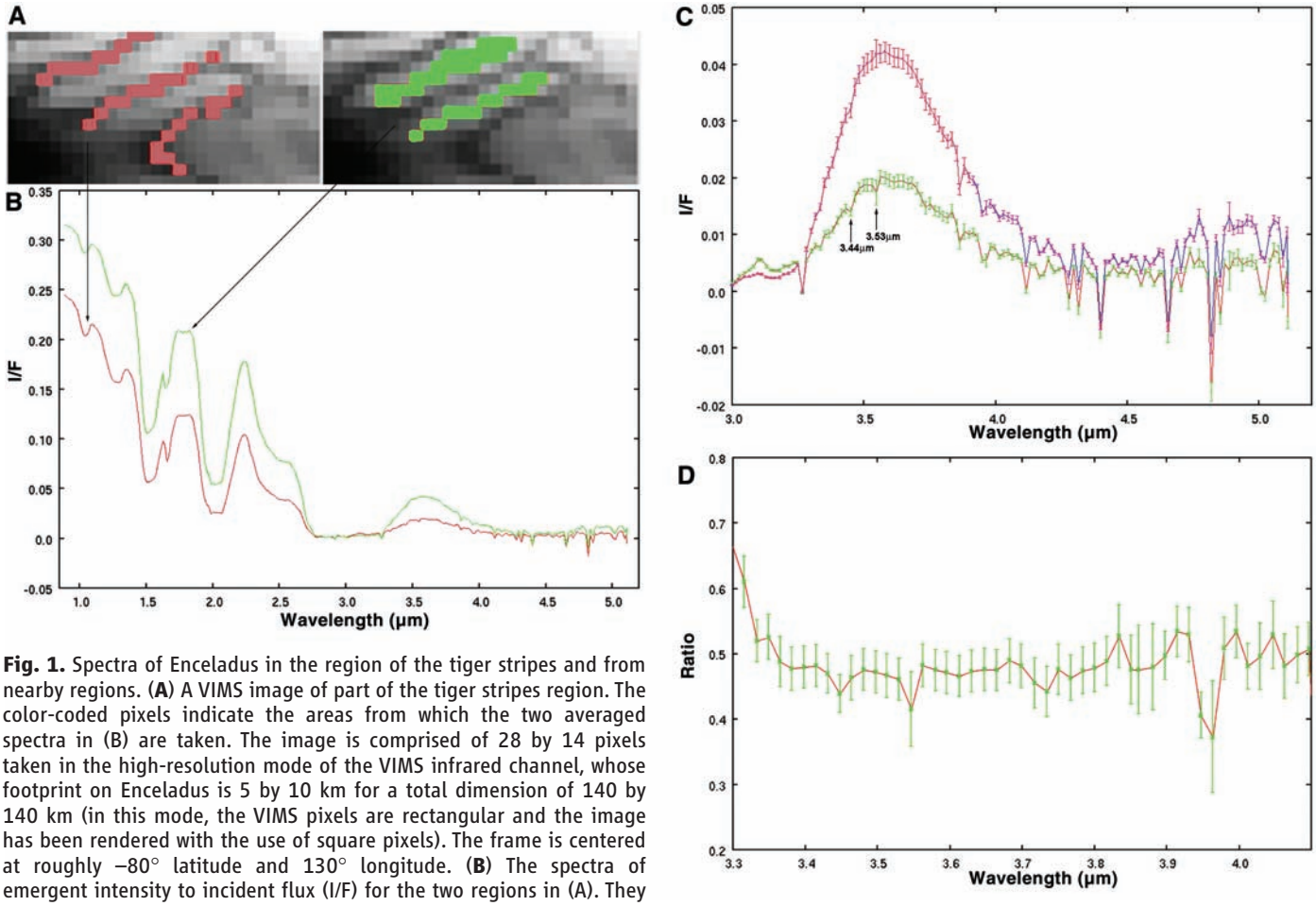


**Fig. 1.** Spectra of Enceladus in the region of the tiger stripes and from nearby regions. (**A**) A VIMS image of part of the tiger stripes region. The color-coded pixels indicate the areas from which the two averaged spectra in (B) are taken. The image is comprised of 28 by 14 pixels taken in the high-resolution mode of the VIMS infrared channel, whose footprint on Enceladus is 5 by 10 km for a total dimension of 140 by 140 km (in this mode, the VIMS pixels are rectangular and the image has been rendered with the use of square pixels). The frame is centered at roughly −80° latitude and 130° longitude. (**B**) The spectra of emergent intensity to incident flux (I/F) for the two regions in (A). They were obtained by averaging all of the individual spectra in the tiger stripes and in the nearby areas [see (A)]. (**C**) A more detailed graph of the 3.0- to 5.1-μm spectral region. (**D**) A more detailed graph of the ratio of the two spectra in (C) in the 3.3- to 4.1-μm spectral region. The 1σ error bars in (D) result primarily from level shifts in the two spectra, a result of the tiger stripes being noticeably darker than the surrounding regions. The actual uncertainty in the spectra is better represented by the point-to-point scatter. We attribute the absorptions near 3.44 and 3.53 μm in the ratio spectrum in (C) to short-chain organics. There are other features in the ratio spectrum that may be real and are, as yet, unidentified. No spectra shown have units. They are simple numerical ratios.

Some telescopic spectra show a weak absorption at 2.2 to 2.4 μm, suggesting the presence of $NH_3$ or $NH_3$ hydrate (*4*, *6*), whereas other spectra of similar quality do not (*5*). The spread in time of the spectra (1995 to 2003) and the change from an equatorial to a more south polar view of Enceladus over that interval suggest the possibility of short-term changes in the surface reflectance. Results of the magnetometer investigation on Cassini gave early indications of a substantial atmosphere on Enceladus (*7*), which led to a lowering of the altitude of the 14 July flyby. The 14 July flyby led to the discovery of a plume of material emanating from the south polar region of Enceladus, most likely from the tiger stripes (the tiger stripes are a complex of volcanically active fissures of likely tectonic origin several hundred kilometers long, concentrated very near the south pole of Enceladus) (*1*, *8*–*10*). Areas within the tiger stripes are substantially hotter than would be expected if only passively heated by sunlight (*8*).

Here, we report near-infrared spectra of spatially resolved regions on Enceladus, which we obtained using the Visible and Infrared Mapping Spectrometer (VIMS) (*11*) during the three Cassini flybys of this satellite in 2005 (17 February, 9 March, and 14 July 2005). In total, 207 VIMS cubes of Enceladus were obtained.

The VIMS is an imaging spectrometer operating in the wavelength region 0.35 to 5.1 μm in 352 channels, with a nominal pixel size of 0.5 mrad and a maximum spatial format of 64 by 64 pixels. The data entity from the instrument is called a "cube" and can be thought of as a stack of 352 images, measuring 64 by 64 pixels and ordered by increasing wavelength.

The analysis of the VIMS data for Enceladus described here is in three general areas: the composition of surface and the size of the ice grains in the near surface, the degree of crystallinity of the near surface, and the temperature of the surface. Although the analysis extends to the entire surface of Enceladus covered by the observations during the three flybys, we focus on the south polar region of Enceladus and particularly on the area of the tiger stripes because they are so unusual.

Our analysis of the spectrum of Enceladus shows that its surface is almost completely dominated by water ice (Fig. 1) with a weak coloring agent in the ultraviolet-visible spectral region and with some minority constituents in specific areas. Globally, the typical water-ice grain size is 50 to

[1]Lunar and Planetary Laboratory, University of Arizona, Tucson, AZ 85721, USA. [2]U.S. Geological Survey, Denver, CO 80225, USA. [3]Jet Propulsion Laboratory, California Institute of Technology, Pasadena, CA 91109, USA. [4]NASA Ames Research Center, Moffett Field, CA 94035, USA. [5]Instituto di Fisica dello Spazio Interplanetario, 0133 Rome, Italy. [6]Instituto di Astrofisica Spaziale, 0133 Rome, Italy. [7]Observatoire de Paris-Meudon, 92195 Meudon Cedex, France. [8]Deutsches Zentrum fuer Luft und Raumfahrt, 12489 Berlin, Germany. [9]Institute d'Astrophysique Spatiale, Universite de Paris, 91405 Orsay Cedex, France. [10]Department of Earth and Space Sciences, University of Washington, Seattle, WA 98195, USA. [11]Department of Astronomy, Cornell University, Ithaca, NY 14853, USA. [12]University of Nantes, 44072 Nantes Cedex, France.

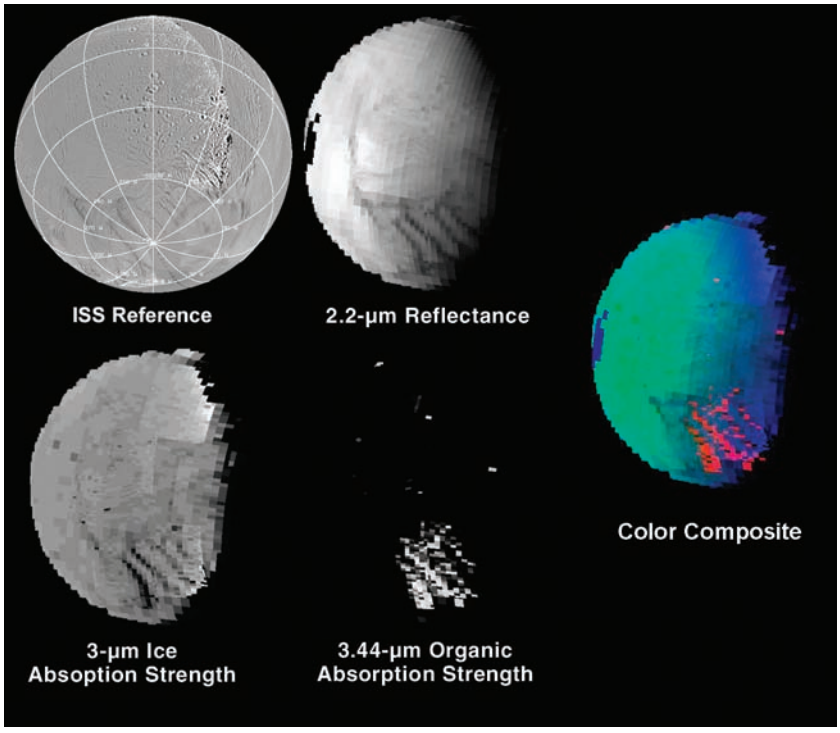


**Fig. 2.** A compositional map of Enceladus. This map was produced by stacking red, green, and blue images coded as follows: The red image maps the strength of the 3.44-μm organic absorption to red intensity, the green image maps the 2.2-μm continuum reflectance to green intensity, and the blue image maps the intensity of the 3-μm water-ice absorption to blue intensity. The images are stacked as a red-green-blue triplet. Note the correlation of the organic signature with the tiger stripes and the presence of stronger water-ice absorptions there as well. ISS, visible-wavelength Imaging Science Subsystem.

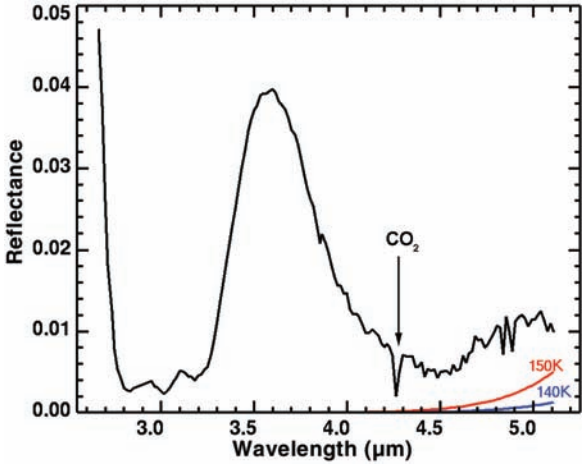


**Fig. 3.** Average spectrum of the tiger stripes. Note the strong $CO_2$ absorption near 4.26 μm. The curves labeled 140 and 150 K are the apparent reflectance that would result for a surface that had a 0.0 actual reflectance at those two temperatures.

150 μm, but grain sizes increase to 100 to 300 μm in the tiger stripes region (Figs. 1 and 2).

We found traces of free $CO_2$ ice, trapped $CO_2$ (either as a liquid or gaseous inclusion), and simple organics in the tiger stripes. Whereas the organic signatures map geologic features (Fig. 2), the close approach data for 14 July have anomalous noise that obscures spectral features with wavelengths longer than 4 μm. CO and $CO_2$ are molecules that we would expect to find in icy bodies formed in the Saturn system (*12*–*17*). Indeed, we found free $CO_2$ ice in small amounts globally and in higher concentrations near Enceladus' south polar regions, but we found no CO.

In data taken well before the closest approach on 14 July 2005, we found in the tiger stripes region a strong signature of $CO_2$ with an absorption-band depth of 74%. The center wavelength of the $CO_2$ absorption in the tiger stripes region indicates that the $CO_2$ is not free ice, but rather complexed, most likely with water ice (Fig. 3). There is no evidence in our data for free $CO_2$ ice in the tiger stripes. This is perhaps not surprising because the temperatures seen there by the Cassini Composite Infrared Spectrometer (CIRS) instrument (*8*) would cause solid $CO_2$ to rapidly migrate northward of the tiger stripes region to areas with colder temperatures. Some free $CO_2$ is indeed seen northward of the tiger stripes region in our data. Furthermore, that there is such a high abundance of complexed $CO_2$ in the tiger stripes suggests active replenishment, probably from ongoing geophysical activity in the region (*1*, *8*–*10*).

No signature of CO ice, gas, clathrate, or any other physical form was seen in our data. Based on the data taken about 1 hour before the closest approach, an upper limit of 5 precipitable nanometers (corresponding to a column density of roughly $10^{14}$ molecules/cm$^2$) can be placed on the amount of CO in the atmospheric column above the tiger stripes.

Another cosmochemically important compound is $NH_3$. The role of $NH_3$ in solar system chemistry and geophysics has been extensively studied, and its role in Enceladus' geophysical activity has been widely hypothesized (*3*, *18*–*22*). Unfortunately, no features due to $NH_3$ or its various hydrates were identified on Enceladus. To derive plausible upper limits for the abundance of $NH_3$ on Enceladus, we considered models of $NH_3$ plus water-ice mixtures. For $NH_3$ grain sizes similar to that of the water ice, we derived an upper limit of ~1%. If the $NH_3$-ice grains on Enceladus are larger than the water-ice grains, our modeling admits upper limits of ~3%. $NH_3$ has its strongest absorptions near strong water-ice absorptions, thus reducing the sensitivity of models where $NH_3$ is intimately mixed with water. It is possible that small areas of pure $NH_3$ exist if they subtend less than 10% of a VIMS pixel, but considering all of this, the likely global upper limit to $NH_3$ on the surface of Enceladus is 2%. It should be noted, however, that as for $CO_2$, temperatures in the area of the tiger stripes may be high enough to cause free $NH_3$ ice to migrate northward to areas of lower temperatures.

There are many other apparent spectral features in the VIMS data for Enceladus that require further study before an accurate assessment of their importance can be made. Of possible particular importance is a downturn in wavelengths longer than 5 μm and a possible 5.0-μm feature in the global average spectrum of Enceladus.

Disk-integrated spectra of Enceladus indicate that the water ice in Enceladus' equatorial and mid- to high-latitude regions is primarily crystalline (*4*, *6*). Nevertheless, amorphous water ice should exist on the satellite (*4*). Amorphous water ice forms when it is condensed directly from the vapor to a solid at temperatures below about 100 K. If amorphous water ice is heated to 150 K, it irreversibly and exothermally

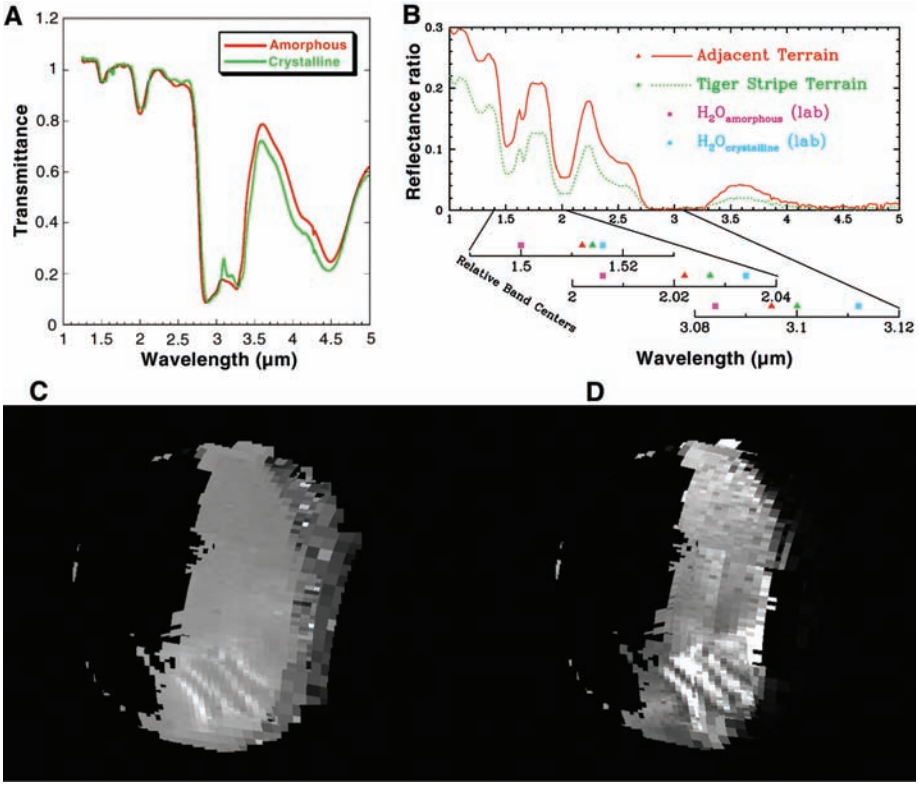


**Fig. 4.** (**A**) Spectra of crystalline and amorphous ice showing the 1.6-μm absorption band and the 3.1-μm Fresnel peak, both characteristic of crystalline ice (*4*). (**B**) Co-added spectra of the tiger stripes and the south polar region between the tiger stripes. Below the graph are the band positions for the main absorption bands at 1.5 and 2.0 μm and the Fresnel peak at 3.1 μm for the tiger stripes, the region between the tiger stripes, and amorphous and crystalline ice. The region with spectral characteristics most similar to crystalline ice is the tiger stripes. (**C**) A ratio of the 1.2-μm continuum to the 1.65-μm crystalline ice absorption band, showing that the tiger stripes have the deepest absorption at 1.65-μm and thus have the highest abundance of crystalline ice. (**D**) A ratio of the 1.2-μm continuum to the 3.1-μm Fresnel peak characteristic of crystalline water ice. The peak is highest in the tiger stripes, which is consistent with a high degree of crystallinity. The dark regions in the left part of the mosaics in (C) and (D) are due to saturated data.

converts on time scales of minutes to hours to crystalline water ice. The conversion can only be reversed by disruption of the crystal structure by bombardment of high-energy particles (*23*)—a process primarily limited by dose rather than by the energy spectrum of the incident particles (*24*). Examples of such a process can be seen on the Galilean satellites (*23*, *25*, *26*).

Enceladus orbits in the inner regions of Saturn's magnetosphere, where the particle flux is quite high. Furthermore, Enceladus may have its own magnetic field (*7*), which could increase the particle flux at its poles; because of this possibility, looking for amorphous ice near Enceladus' poles would be prudent.

Differences in their spectra can be exploited to search for crystalline and amorphous water ice on Enceladus (Fig. 4). The two most obvious indicators are the 1.65-μm absorption band and the 3.1-μm Fresnel reflection peak, both of which are much more prominent in crystalline ice. In addition, the central wavelengths of the absorption bands vary substantially between amorphous and crystalline water ice because of the reduced hydrogen bonding in amorphous water ice compared with that in crystalline ice (Fig. 4B). Our analysis indicates that, in a local sense (that is, confining our analysis to the south polar regions of Enceladus), crystalline ice is most abundant in the tiger stripes, whereas amorphous ice is most abundant in the south polar regions outside the tiger stripes. This is shown in the global ratio of the 1.2-μm reflectance to the 1.65-μm absorption band (Fig. 4C) and in the ratio of the 1.2-μm reflectance to the 3.1-μm peak (Fig. 4D), except that the tiger stripes are darker because the crystalline ice is brighter at 3.1 μm.

Laboratory experiments show that crystalline ice at temperatures below 100 K rapidly converts to amorphous ice in the presence of high-energy particles (*24*) and recrystallizes very quickly when heated to ~140 to 150 K (*23*). For geologically active, relatively hot areas such as those near Enceladus' south pole, it would be difficult, if not impossible, to determine the time that these materials have been exposed to magnetospheric bombardment—i.e., their age. If, on the other hand, areas with a high degree of crystallinity exist in the coldest areas in the south polar region of Enceladus, they would be young, perhaps as young as a few decades (*24*). Further study of our data and additional observations of Enceladus' south polar region are required to address the question of age.

Despite the unambiguous detection of anomalously hot areas on Enceladus by the Cassini CIRS instrument (*8*), VIMS did not detect thermal emission from within the tiger stripes, mostly because the cutoff wavelength of the instrument is 5.1 μm. Co-adding spectra of the stripes to improve the signal-to-noise ratio allows us to place a robust 3σ upper limit at 140 K on the average temperature of VIMS tiger stripes pixels (*27*). Alternatively, a swath within the stripes can neither be wider than 135 m at the ammonia-water eutectic temperature of 173 K nor wider than ~20 cm at the water triple point 273 K.

## References


1. C. C. Porco *et al.*, *Science* **311**, 1393 (2006).
2. W. B. McKinnon, *Rev. Geophys.* **25**, 260 (1987).
3. J. S. Kargel, S. Pozio, *Icarus* **119**, 385 (1996).
4. W. M. Grundy, M. W. Buie, J. A. Stansberry, J. R. Spencer, B. Schmitt, *Icarus* **142**, 536 (1999).
5. D. P. Cruikshank *et al.*, *Icarus* **175**, 268 (2005).
6. J. P. Emery, D. M. Burr, D. P. Cruikshank, R. H. Brown, J. B. Dalton, *Astron. Astrophys.* **435**, 353 (2005).
7. M. K. Dougherty *et al.*, *Science* **311**, 1406 (2006).
8. J. R. Spencer *et al.*, *Science* **311**, 1401 (2006).
9. C. J. Hansen *et al.*, *Science* **311**, 1422 (2006).
10. J. H. Waite Jr. *et al.*, *Science* **311**, 1419 (2006).
11. R. H. Brown *et al.*, *Space Sci. Rev.* **115**, 111 (2005).
12. J. S. Lewis, *Icarus* **15**, 174 (1971).
13. J. S. Lewis, *Science* **172**, 1127 (1971).
14. J. S. Lewis, *Sci. Am.* **230**, 51 (1974).
15. J. S. Lewis, *Annu. Rev. Phys. Chem.* **24**, 339 (1973).
16. J. S. Lewis, R. G. Prinn, *Astrophys. J.* **238**, 357 (1980).
17. J. S. Lewis, *Science* **186**, 440 (1974).
18. D. J. Stevenson, in *Uranus and Neptune, NASA Conference Publication 2330*, J. Bergstrahl, Ed. (NASA Scientific and Technical Information Branch, Washington, DC 1984), pp. 405–424.
19. D. J. Stevenson, *Nature* **298**, 142 (1982).
20. S. W. Squyres, R. T. Reynolds, P. M. Cassen, S. J. Peale, *Icarus* **53**, 319 (1983).
21. J. S. Kargel, *Earth Moon Planets* **67**, 101 (1995).
22. R. G. Prinn, B. Fegley, *Astrophys. J.* **249**, 308 (1981).
23. G. B. Hansen, T. B. McCord, *J. Geophys. Res. Planets* **109**, 1012 (2004).
24. G. Strazzulla, G. A. Baratta, G. Leto, G. Foti, *Europhys. Lett.* **18**, 517 (1992).
25. M. G. Kivelson *et al.*, *Nature* **384**, 537 (1996).
26. G. Schubert, K. K. Zhang, M. G. Kivelson, J. D. Anderson, *Nature* **384**, 544 (1996).
27. To establish upper limits on temperature, we used a Levenberg-Marquardt algorithm to fit the co-added tiger stripes spectrum to the spectrum of the interstripe region with the use of a multiplicative albedo-surrogate scaling factor and surface temperature as free parameters. The best fit temperature is indistinguishable from 0 K. We then increased the temperature of either the full pixel or a linear swath through the pixel until the quality of the fit degraded to the 3σ level and used that value for the upper limit.


6 October 2005; accepted 16 January 2006
10.1126/science.1121031